

# PHYSICAL INSIGHT INTO FUEL MIXING ENHANCEMENT WITH BACKWARD-FACING STEP FOR SCRAMJET ENGINES VIA MULTI-OBJECTIVE DESIGN OPTIMIZATION

H. Ogawa\*, C. Y. Wen<sup>†</sup>, Y. C. Chang<sup>‡</sup>

\*School of Aerospace, Mechanical and Manufacturing Engineering, RMIT University, Melbourne, Australia

<sup>†</sup>Department of Mechanical Engineering, The Hong Kong Polytechnic University, Kowloon, Hung Hom, Hong Kong

<sup>‡</sup>Department of Aeronautics and Astronautics, National Cheng Kung University, Tainan, Taiwan

**Keywords:** Fuel injection, Backward-facing step, CFD, Evolutionary algorithms, Surrogate modeling

## Abstract

Fuel injection into crossflow behind a backward-facing step is studied by means of multi-objective design optimization, aiming at fuel/air mixing for supersonic combustion of scramjet propulsion. A variety of injector configurations have been examined in the optimization process using evolutionary algorithms in conjunction with local search methods and surrogate modeling. Data mining has been performed by applying statistical techniques including variance-based sensitivity analysis to the surrogate models constructed with solutions from computational fluid dynamics. The injection angle and backward step height have been found to be the most influential design parameters on the mixing performance for the configurations considered in this study.

## 1 Introduction

Hypersonic air-breathing propulsion offers the potential for reliable and economical transport for access to space and high-speed atmospheric flight. In particular, scramjet (Supersonic Combustion Ramjet) propulsion is a promising technology that can enable efficient and flexible transport systems by removing the need to carry oxidizers and other limitations of conventional rocket engines. The last decade has seen remarkable milestones achieved by various flight exper-

iments including The University of Queensland's HyShot II in 2002[1, 2], the NASA X-43 vehicles in the Hyper-X program in 2004[3], and the Boeing X-51A WaveRider in 2010[4].

The scramjet mechanism critically depends on the sequential process – capture and compression of hypersonic airflow in the inlet, fuel injection into the air, supersonic combustion in the chamber, and expansion of combustion products through the nozzle for thrust. Fuel injection plays a major role in the flow process, responsible for efficient combustion and hence overall scramjet performance[5]. The airflow slows down from hypersonic to supersonic through the inlet, but further deceleration would lead to undesirable high static temperature and result in limited heat release due to excessive dissociation of nitrogen and oxygen gases[6]. The interactions between fuel and air including mixing, ignition and combustion occur at an extremely short timescale, rendering the development of efficient and reliable fuel injection systems of crucial importance.

The significance of fuel injection in airbreathing engines has brought about a considerable number of mixing techniques. Examples include: traverse/tangential injection through wall orifices[7, 8, 9], streamwise vortices with alternating wedges (hypermixers)[10, 11], shock-enhanced mixing with alternative compression ramps and expansion troughs[12], and backward

transverse/inclined injection in the vicinity of a backward-facing step or a cavity[13, 14, 15, 16]. The last method, in particular, offers advantages in various aspects, in particular, self ignition and flame holding in the recirculation zone downstream of the step, where injected fuel is mixed with relatively slow airflow at high temperature.

A recent shock-tunnel experiment conducted by the authors observed strong interactions between recombination shock waves due to the reattachment of the separated shear layer and the inclined fuel jet adjacent to the reattachment point downstream of a backward-facing step (Fig. 1)[17]. The flow visualization via high-speed Schlieren suggested promising effects of the jet interactions on fuel/air mixing enhancement owing to the baroclinic torque induced by misaligned pressure gradient in conjunction with shear-induced Kelvin-Helmholtz vorticity. Former research efforts on fuel injection with a backward step have been made, with primary focus on the jet interactions and mixing characteristics for prefixed configurations[13, 14, 15, 16, 17], and no preceding research has studied geometric effects on the mixing performance systematically, to the knowledge of the authors.

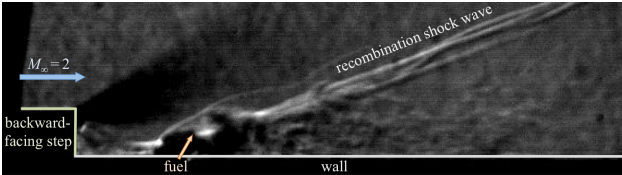


**Fig. 1** Interactions of recombination shock waves with fuel injected into supersonic crossflow behind a backward-facing step[17]

The present numerical study is undertaken to investigate the effects of the design parameters on the fuel/air mixing by means of multi-objective design optimization (MDO) using surrogate-assisted evolutionary algorithms coupled with computational fluid dynamics, which has been applied extensively to numerous optimization problems for scramjet engines[18, 19, 20]. The results from are examined by covariance-based sensitivity analysis using surrogate prediction to extract essential information on key design factors for this fuel mixing method. Flowfields

are visualized and scrutinized for representative configurations in comparison with the reference geometry in order to elucidate underlying flow physics that is responsible for the fuel behavior and mixing characteristics.

## 2 Approaches

### 2.1 Configurations and Conditions

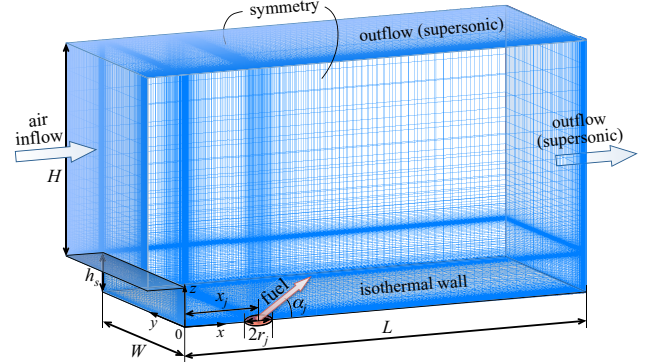


**Fig. 2** Schematic of fuel injection into air crossflow downstream of a backward-facing step

The configuration considered in this study is schematically presented in Fig. 2, as per the settings experimental setups[17]. The flow conditions considered in this study are shown in Table 1 in terms of the Mach number ( $M$ ), static and total pressures ( $p$  and  $p_0$ ), and static and total temperatures ( $T$  and  $T_0$ ), assuming sonic fuel injection into airflow incoming at Mach 2 with a dynamic pressure of 418 kPa and Reynolds number of  $1.43 \times 10^7$  per unit length. Methane ( $\text{CH}_4$ ) is used as fuel to be injected into crossflow of air, where both gases are assumed to be calorically perfect with a specific heat ratio  $\gamma$  of 1.32 and 1.4, respectively, in the present study. The fuel injection pressure  $p_j$  is adjusted according to the injector radius  $r_j$  to maintain the jet-to-freestream momentum flux ratio  $J \left( \equiv \frac{(\rho V^2)_j}{(\rho V^2)_\infty} \right)$  at 1.43.

**Table 1** Crossflow air and fuel injection conditions

	$M$	$p$ [kPa]	$p_0$ [kPa]	$T$ [K]	$T_0$ [K]
Air	2	150	1174	1100	1980
Fuel	1	910	7003	259	425

The floor is taken to be an isothermal wall, with the temperature maintained at 300 K for a

short test time in the impulse facility, as shown in Fig. 2, which displays the boundary conditions used in this paper. It also depicts the four design parameters, namely, the angle  $\alpha_j$ , stream-wise position  $x_j$ , and radius  $r_j$  of the fuel injector as well as the height of the backward-facing step  $h_s$ . The length ( $L$ , after the step), width ( $W$ ), height ( $H$ ) of the computational domain are fixed at 0.055 m, 0.02 m, 0.032 m, respectively, in concordance with the experimental setups[17]. The domain also include a 5 mm trailing-edge of the backward step at a height of  $h_s$ . Imposed at its entrance as an inflow is the profile of a turbulent boundary layer, which has grown over 30 mm from the leading edge of a flat plate, as per the experimental arrangement.

## 2.2 Computational Fluid Dynamics

Compressible flowfields in the presence of fuel injection are computed by utilizing a commercial solver CFD++ [22], which has been employed by the Australian hypersonics network for scramjet research due to its demonstrated fidelity in hypersonic aerodynamics[18, 19, 20]. An implicit algorithm with second-order spatial accuracy is used to solve the Navier-Stokes equations for viscous flowfields and convergence is accelerated by the multigrid technique. The boundary layer is taken to be fully turbulent and modeled by the two-equation SST  $k$ - $\omega$  RANS model. Steady flowfields are computed in the present study, which focuses on fuel/air mixing purely due to steady fluid dynamics and interactions, excluding effects of unsteady phenomena such as shear-induced vorticity motion.

Three-dimensional computational meshes are generated automatically by Glyph scripting on a commercial grid generator Pointwise[23] for the fuel injection configuration represented by the four design variables introduced in the former section. A fully structured mesh comprising 1,275,000 cells are generated for each configuration, based on the topology and mesh sensitivity study described in the preceding studies[20, 21]. The computational mesh is superimposed in Fig. 2 for the baseline geometry, which corresponds to the experimental model[17].

## 2.3 Multi-Objective Design Optimization

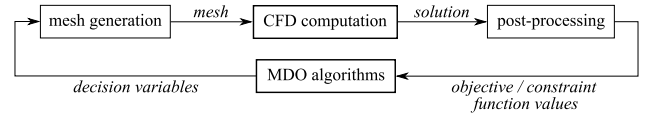


Fig. 3 Optimization chain

In order to conduct a design optimization for the injector in a coupled MDO/CFD approach, a process chain is set up and implemented, consisting of mesh generation (pre-processing), CFD computation (evaluation), post-processing and optimization algorithms, as schematically shown in Figure 3. Design optimization is performed by applying evolutionary algorithms, in particular, the elitist non-dominated sorting genetic algorithm (NSGA-II)[24, 25]. It is a population-based approach that evolves the candidate solutions in the population pool over generations, enabling global search. Simulated binary crossover and polynomial mutation are used as recombination operators at a given probability (1.0 and 0.1, respectively, in this study) with a specified distribution index (10 and 20, respectively).

Multiple surrogate models including response surface models, radial basis function networks, kriging and multilayer perceptrons, are employed to mitigate the computational cost by replacing the CFD evaluations[26], trained regularly (every 5 generations in this study). Once surrogate models become available, hybrid (memetic) optimization is performed by incorporating local search methods including pattern search and sequential quadratic programming combined with adaptive weighting into evolutionary algorithms[27, 28]. Covariance-based global sensitivity analysis[29, 30] is applied to the solution archive resulting from CFD evaluations so as to investigate the effects of the decision variables (input parameters) on the objective functions (objective functions).

## 2.4 Design Criteria

The performance of fuel injection is evaluated by quantifying the resultant flowfields with respect to multiple criteria. High total pressure recovery is a desired feature in fuel mixing so as to enable

effective combustion and high thrust production. This objective is targeted by minimizing the total pressure loss defined as  $\Delta p_0 \equiv 1 - \frac{\int_x p_0 d\dot{m}}{\int_{x=0} p_0 d\dot{m}}$ . Fuel penetration into the crossflow is another important characteristic of fuel injection. This criterion is assessed by the penetration height defined as  $h_p \equiv \max(z | c_{\text{CH}_4} > 0.1 c_{\text{CH}_4}^s)$  at the exit, where  $c_{\text{CH}_4}$  and  $c_{\text{CH}_4}^s$  are the fuel mass fraction and its stoichiometric value (0.0548), respectively. It evaluates the fuel remaining in the mainstream without being captured in the recirculation region behind the backward step.

The mixing efficiency is commonly used to evaluate the mixing ability of transverse fuel injection by examining the fuel massflow with respect to the stoichiometric ratio for the outflow, but it is not deemed as a suitable criterion for the current configuration, where the recirculation zone plays a major role in fuel mixing and flame holding (in case of ignition and combustion). The fuel massflow deficit is thus considered in this study, defined as  $\Delta \dot{m}_f \equiv 1 - \frac{\int_x d\dot{m}_f}{\int_{x=0} d\dot{m}_f}$ , where  $\dot{m}_f$  is the fuel massflow rate. The non-dimensionalized streamwise circulation is employed as the last metric to account for the overall effects of streamwise vortices, which plays a primary role in the fuel/air mixing[5, 12]. It is defined as:  $\Gamma \equiv \frac{1}{u d} \int_x |\omega_x| dA$ , where  $\omega_x$  is the streamwise vorticity,  $u$  the crossflow velocity and  $d$  the effective injector diameter (1330 m/s and 1 mm, respectively).

## 2.5 Optimization Problem

Multi-objective design optimization is performed with these parameters, aiming to minimize  $\Delta p_0$  and maximize  $h_f$  simultaneously. The geometric parameters introduced in Section 2.1 are employed as the decision variables. The optimization problem statement of this study is expressed as:

$$\begin{aligned} &\text{minimize:} && \Delta p_0 \\ & && -h_f \\ &\text{subject to:} && 30^\circ \leq \alpha_j \leq 90^\circ \\ & && 0.005 \text{ m} \leq x_j \leq 0.015 \text{ m} \\ & && 0.0003 \text{ m} \leq r_j \leq 0.001 \text{ m} \\ & && 0.0025 \text{ m} \leq h_s \leq 0.01 \text{ m} \end{aligned}$$

## 3 Results

### 3.1 Design Optimization

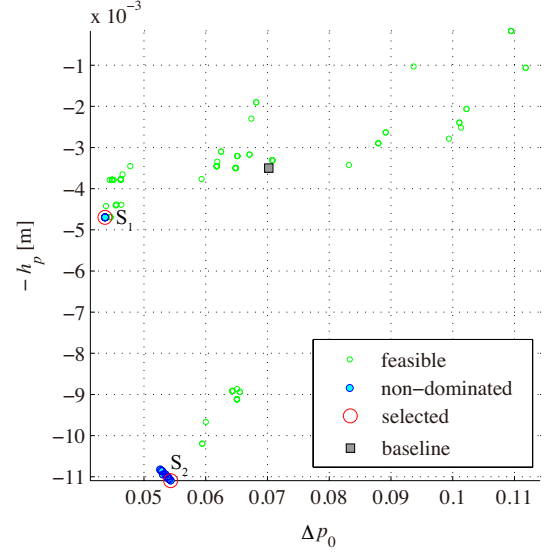


**Fig. 4** Optimization results with CFD evaluations ( $N = 12$ , 10<sup>th</sup> generation)

An MDO coupled with CFD has been performed over 10 generations with a population size of  $N = 12$ , primarily to obtain a minimal number of flow solutions that allows surrogate models to be trained for post analysis within the constraints of time and resources. The distribution of all individuals evaluated in the course of this run is displayed in Fig. 4, along with the non-dominated and representative configurations.

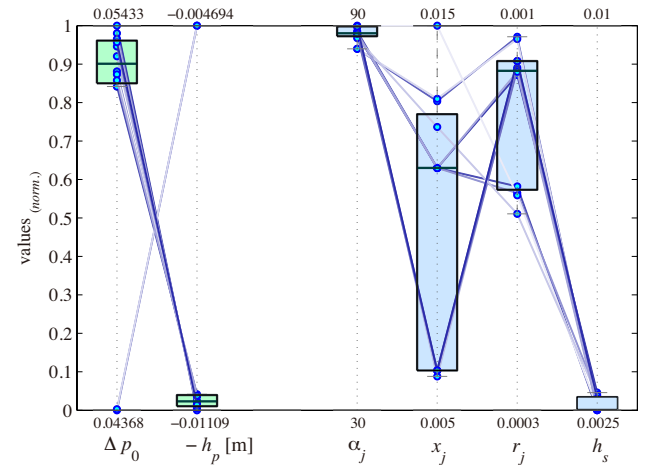


**Fig. 5** Distributions of performance and design parameters with CFD evaluations

The correlations of the performance and de-

sign parameters (objective functions and decision variables) are shown as a parallel coordinate plot in Fig. 5 for all non-dominated solutions evaluated with CFD. A trade-off tendency between total pressure saving and fuel penetration is suggested by the fact that lines connecting corresponding values of  $\Delta p_0$  and  $-h_f$  intersect near the center point within their ranges. The lines for the decision variables indicate that the non-dominated configurations are commonly characterized by large injection angle ( $\alpha_j$ ) and low height of the backward step ( $h_s$ ) close to their upper and lower bounds, respectively, whereas they are less decisive on the injector location ( $x_j$ ) and radius ( $r_j$ ), as seen by scattered distributions.

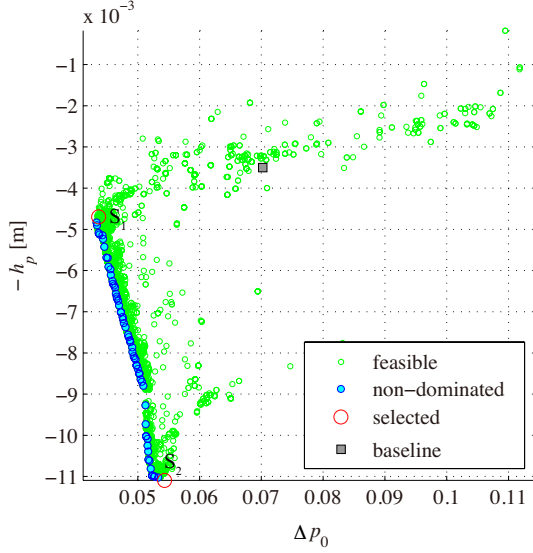


**Fig. 6** Optimization results with surrogate prediction ( $N = 60$ , 50<sup>th</sup> generation)

An additional full-scale MDO has been performed over 50 generations with a population size of  $N = 60$ , using estimation from surrogate models with the best accuracy in lieu of CFD simulations (the mean square error for the prediction of  $\Delta p_0$  and  $h_f$  is 2.67% and 8.16%, respectively, with the kriging model). The resultant distribution plotted in Fig. 6 indicates the presence of a well-defined Pareto optimal front comprising the non-dominated individuals.

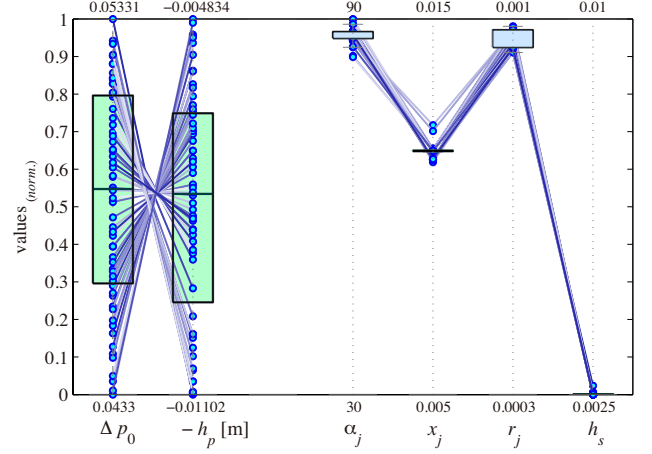


**Fig. 7** Distributions of performance and design parameters with surrogate prediction

Figure 7 displays the correspondence between the objective functions and decision variables in the form of a parallel coordinate plot for all non-dominated individuals from surrogate prediction. A counteracting nature of the total pressure and fuel penetration is evident with the intersecting lines. A bundle of lines linking the decision variables suggest that the non-dominated configurations are associated with unique combinations of these variables about  $\alpha_j \approx 90^\circ$ ,  $x_j \approx 11.5$  mm,  $r_j \approx 1$  mm, and  $h_s \approx 2.5$  mm, in contrast to the MDO results from CFD (Fig. 5), where  $x_j$  and  $r_j$  were more flexible.

### 3.2 Data Reduction

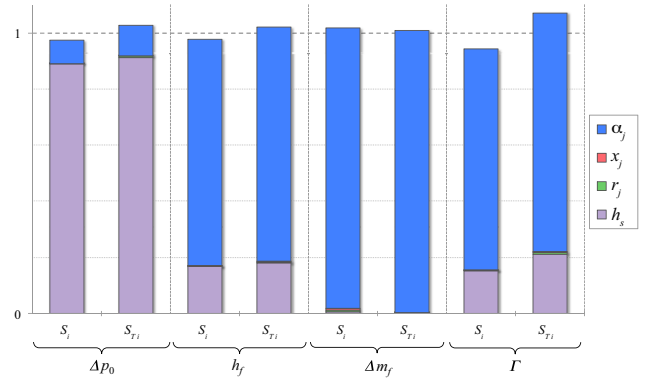
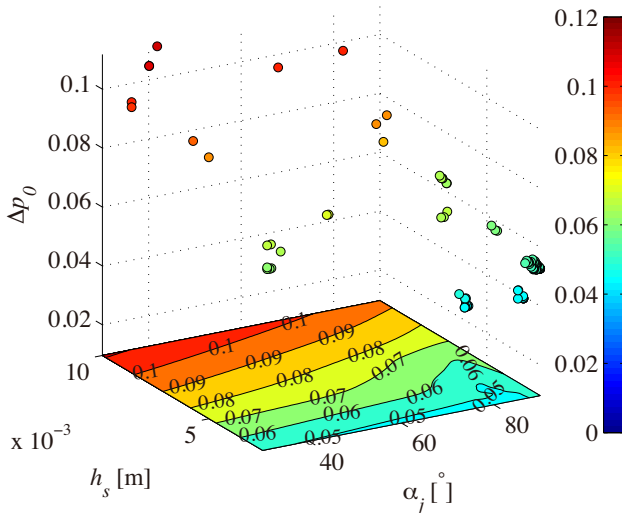


**Fig. 8** Sensitivity indices

Statistical techniques have been applied to the optimization results so as to extract useful knowledge effectively. Figure 8 displays the sensitivity indices obtained with surrogate prediction for

10,000 sample data points. The first-order ( $S_i$ ) and total-effect ( $S_{T_i}$ ) indices from the input parameters ( $\alpha_j$ ,  $x_j$ ,  $r_j$ , and  $h_s$ ) are plotted for the output parameters, *i.e.*, objective functions ( $\Delta p_0$  and  $h_f$ ) and additional design criteria, that is, the fuel massflow deficit  $\Delta \dot{m}_f$  and streamwise circulation  $\Gamma$  (for which the best prediction is given by the kriging with *m.s.e.* of 3.03% and 4.40%, respectively). It is seen that all output parameters are predominantly influenced by two parameters, namely, the injection angle  $\alpha_j$  and backward step height  $h_s$ , with minor or negligible influence of the other two parameters ( $x_j$  and  $r_j$ ).

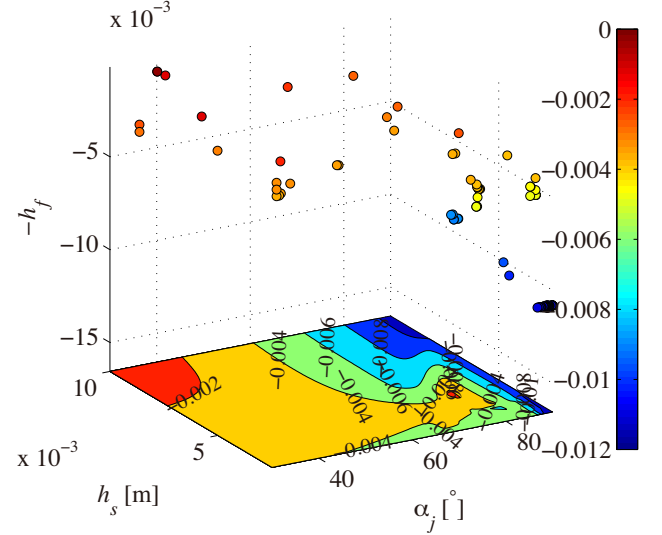
Further data mining has been performed, with particular focus on the impact of these two dominant design parameters. Figures 9-12 display the variations of the output parameters in response to these two input parameters. The colored dots represent the values from all CFD solutions, whereas the floor contours are based on surface fitting of surrogate-predicted points via linear least squares with 10%-span robust bi-square weighting (the R-squared values are shown in the captions).



**Fig. 9** Total pressure loss variation ( $R^2 = 0.977$ )

In Fig. 9,  $\Delta p_0$  increases almost linearly as the step height  $h_s$  increases. The injection angle  $\alpha_j$  has rather minor influence, but it is interesting to note that larger total pressure is incurred at lower injection angles, opposite to the tendency commonly observed in transverse injection studies[31]. This may partly be due to the fact that a higher injection angle causes a larger

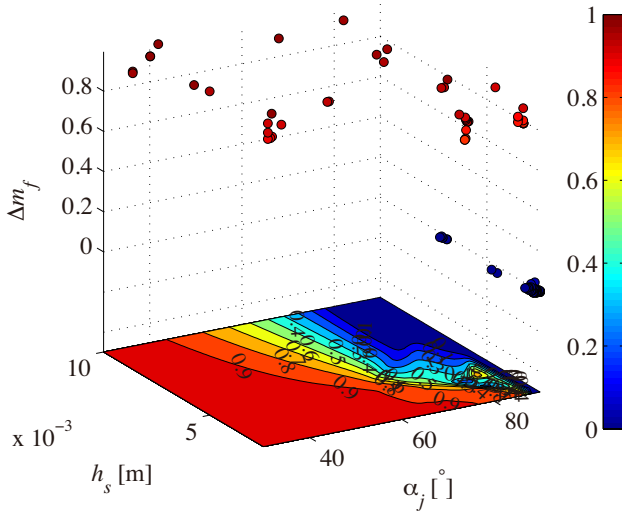
amount of fuel with a higher total pressure (as seen in Table 1) carried downstream to the exit, which effectively compensates the total pressure loss from a stronger bow shock.



**Fig. 10** Fuel penetration height variation ( $R^2 = 0.944$ )

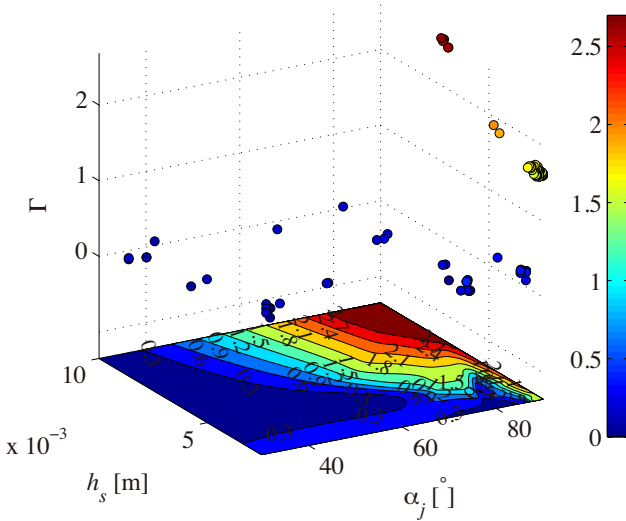
On the other hand, higher fuel penetration  $h_f$  at the exit is achieved with higher injection angles (Fig. 10). The contour suggests that large step heights tend to be associated with greater fuel penetration on the whole, but this trend is somewhat blurred near the lower bound of the injection angle ( $\alpha_j \approx 30^\circ$ ) as well as the lower height limit ( $h_s \approx 2.5$  mm).

Figure 11 indicates substantial changes in the fuel massflow deficit with the increase in both injection angle and backward step height. It suggests that the portion of the fuel poured into in the recirculation zone decreases at higher injection angles and that the injection angle exerts influence on the pooled fuel amount over a wider range with higher backward steps. It is notable that most fuel remains in the recirculation zone ( $\Delta \dot{m}_f \approx 1$ ), with little influence of the injection angle (except high angles  $\alpha_j \approx 90^\circ$ ) at low step heights ( $h_s \approx 2.5$  mm).



**Fig. 11** Fuel massflow deficit variation ( $R^2 = 0.848$ )

Figure 12 shows considerable dependency of the streamwise circulation on the two design parameters. In particular,  $\Gamma$  increases drastically in the vicinity of normal injection ( $\alpha_j \approx 90^\circ$ ). It grows further with larger backward step heights, associated with enhanced generation of streamwise vortices, while there is a little ambiguity near the lower bound ( $h_s \approx 2.5$  mm) especially at high injection angles ( $\alpha_j \approx 90^\circ$ ).



**Fig. 12** Streamwise circulation variation ( $R^2 = 0.841$ )

In order to probe into the tendencies observed above, two individuals among all solutions evaluated with CFD are selected to represent the superior individuals with respect to the two objective functions, denoted as  $S_1$  and  $S_2$ , as plotted

in Figs. 4 and 6. The design parameters of these geometries are shown in Table 2 and compared in Fig. 13, along with the output parameters.

**Table 2** Design parameters of baseline and selected configurations

	$\alpha_j$ [°]	$x_j$ [mm]	$r_j$ [mm]	$h_s$ [mm]
baseline	60.0	10.0	1.00	5.00
$S_1$	86.4	13.0	0.98	2.50
$S_2$	88.7	11.3	0.91	2.85

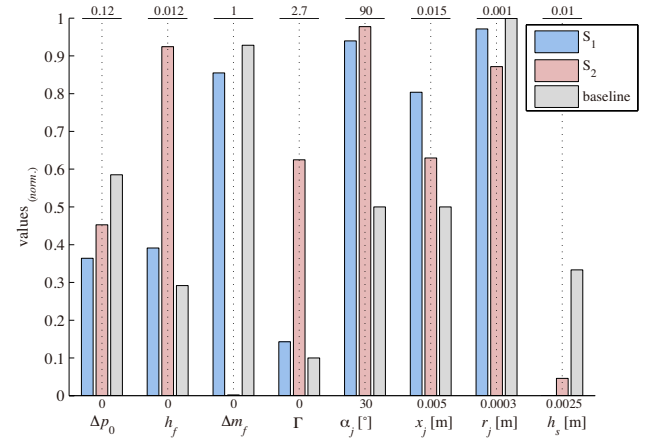
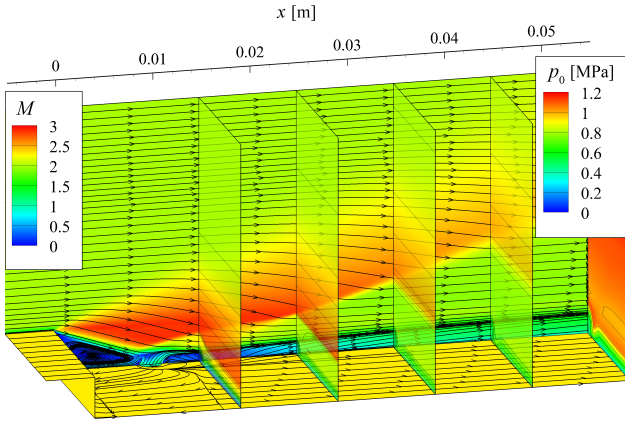


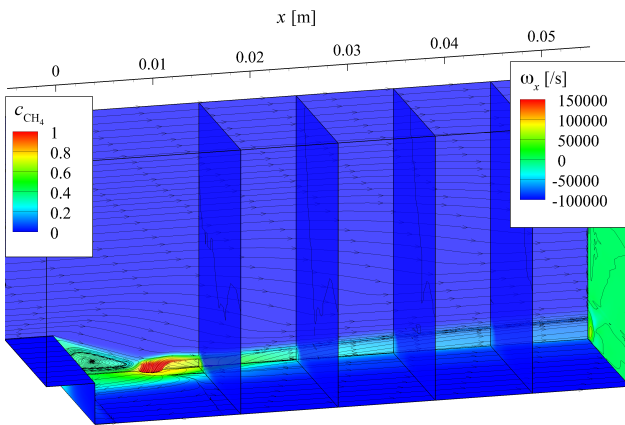
**Fig. 13** Comparison of performance and design parameters for representative configurations

### 3.3 Flowfields

The flowfields associated with the baseline and selected configurations are plotted in Figs. 14-16. The first image of each figure set displays the Mach number distributions on the symmetry plane ( $y = 0$  m) and cross sections with an equal interval of 0.05 m, except on the exit plane ( $x = 0.055$  m), where the total pressure distribution is plotted instead for the evaluation of the total pressure recovery. Streamlines are plotted on the symmetry plane, based on the velocity components ( $u$  and  $w$ ), while those plotted on the floor are based on the surface shear stress ( $\tau_x$  and  $\tau_z$ ). The second image shows the distributions of the fuel mass fraction on the symmetry and floor planes as well as equally-spaced streamwise stations, except at the exit plane, where the streamwise vorticity is plotted instead to allow the examination of the streamwise circulation.



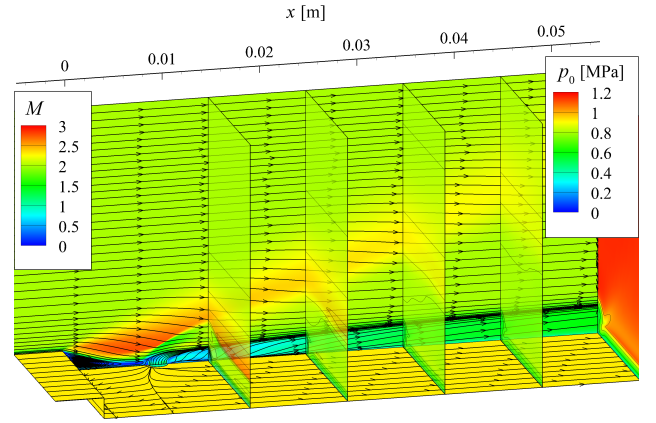
(a) Mach number



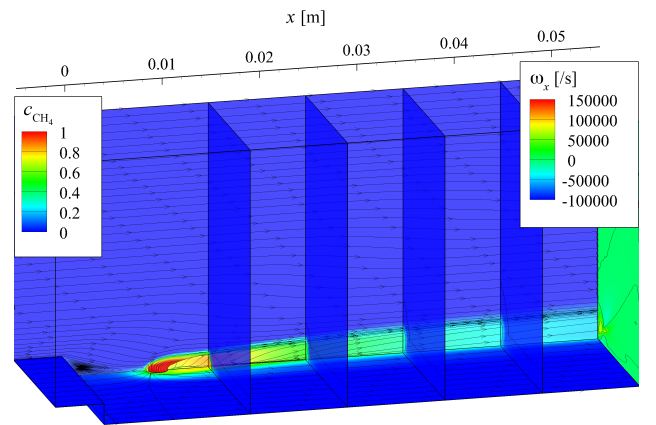
(b) fuel mass fraction

**Fig. 14** Flowfields of baseline configuration

Figure 14 shows the flowfield due to the baseline configuration, corresponding to the Schlieren visualization in Fig. 1 from a shock-tunnel experiment[17]. The Mach number distribution and streamlines plotted on the symmetry plane in Figure 14 (a) indicate the presence of a fuel core stream that locally propagates in a region around the centerline, as well as the effects of the fuel injection that takes place near the downstream end of the recirculation region. The floor streamlines are indicative of fairly localized influence of fuel injection bounded in the vicinity of the symmetry plane. The fuel mass fraction distributions in Fig. 14 (b) also suggests rather localized fuel propagation predominantly in the recirculation zone closer to the symmetry plane. Consequently little fuel is contained in the outflow at the exit, where rather weak streamwise vorticity is observed.



(a) Mach number

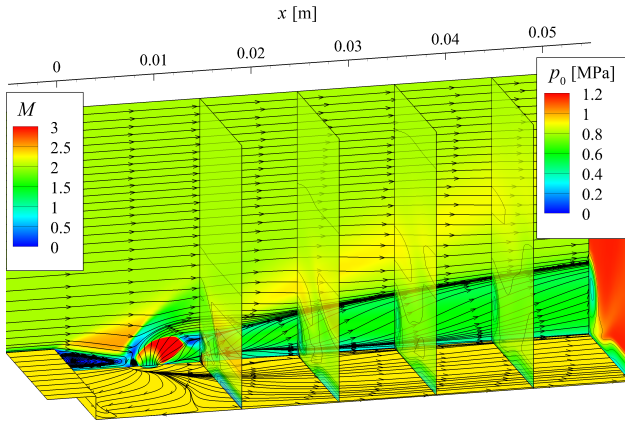


(b) fuel mass fraction

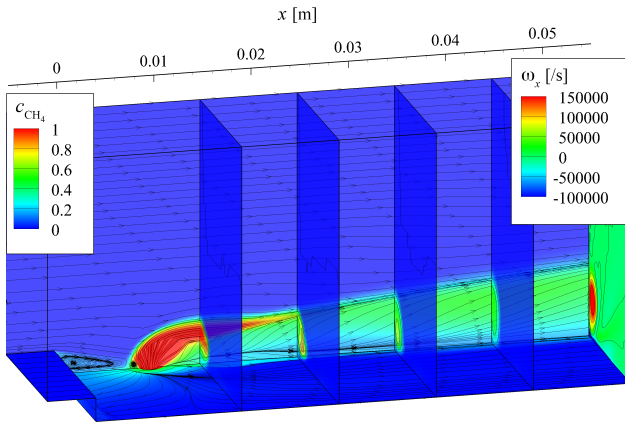
**Fig. 15** Flowfields of  $S_1$  configuration

The  $S_1$  configuration is characterized with a higher injection angle, downstream injector position, and a half step height, as compared to the baseline geometry. The injector is located downstream of the nominal end of the recirculation zone in contrast to the baseline case, as seen in the floor streamlines in Fig. 15 (a). In spite of these differences in the geometric arrangements, however, the major characteristics of the flowfield appear to be similar to those observed with the baseline injector as a whole, in terms of the extent of the jet-crossflow interactions. The fuel mass fraction distributions plotted in Fig. 15 (b), on the other hand, reveal a different behavior of the injected fuel in the recirculation zone, where its propagation appears to be rather inactive, in comparison with the baseline case according to the fuel distributions on the symmetry and floor

planes. This difference, however, has resulted in a rather small decrease in the fuel massflow deficit (Fig. 13), suggesting a large portion of the fuel remains in recirculation, off the symmetry plane and floor wall. A considerably higher total pressure recovery is achieved at the exit with this configuration, which may be attributed primarily to a moderate shock loss due to a lower backward step height and secondarily to a slightly increased fuel massflow, which possesses higher total pressure than the airflow (as seen in Table 1).



(a) Mach number



(b) fuel mass fraction

**Fig. 16** Flowfields of  $S_2$  configuration

The  $S_2$  configuration is also characterized with a high injection angle and low step height, similarly to the  $S_1$  configuration, but features a relative injector position that is similar to the baseline geometry, in that the fuel injector is submerged in the recirculation region. The resultant

flowfield in Fig. 16(a), however, reveals a distinctly different flow structure characterized by various features typically observed in transverse fuel injection into supersonic crossflow such as the presence of a supersonic region within the under-expanded jet bounded by a barrel shock and Mach disk[31]. This characteristic flowfield, similar to that observed experimentally by Kuratani *et al.*[15], can be attributed to the relatively strong injection at a near-normal angle, which penetrates the recirculation zone and reaches out to the main airstream, where the corner expansion around the backward-facing step is not too immense for the resultant bow shock to suppress the growth of the fuel jet at the interface, in contrast with the baseline case in Fig. 14(a). As a consequence a large portion of the fuel is injected into the outer crossflow and mixed with the air owing to strong counter-rotating streamwise vortices, as seen in Fig. 16(b). A small fraction of the injected fuel is fed into the recirculating flow in this case, resulting in virtually no fuel massflow deficit measured at the exit (Fig. 13).

### 3.4 Summary

Key insights obtained in this study are summarized in Table 3 with respect to the effects of the major design parameters, *i.e.*, injection angle and step height, on the performance parameters:

**Table 3** Effects of major design parameters

	$\Delta p_0$	$h_f$	$\Delta \dot{m}_f$	$\Gamma$
$\alpha_j \uparrow$	$\downarrow$	$\uparrow$	$\downarrow$	$\uparrow$
$h_s \uparrow$	$\uparrow$	—	$\downarrow$	$\uparrow$

## 4 Conclusions

A multi-objective design optimization has been performed for methane injected into crossflow downstream of a backward-facing step located in supersonic freestream at Mach 2, assuming fuel injection and mixing for supersonic combustion in scramjet engines. Hybrid optimization approaches combining evolutionary algorithms and local-search methods assisted by surrogate modeling have been applied to the fuel injector design, coupled with high-fidelity computational

fluid dynamics. Four design parameters are employed as the decision variables, namely, the injector angle, streamwise position, and hole radius, as well as the height of the backward step. The total pressure loss and fuel penetration height are used as the objective functions to be minimized and maximized, respectively. Sensitivity analysis has been applied to these parameters along with other two design criteria, that is, the fuel massflow deficit and streamwise circulation. Injection flowfields have been scrutinized for selected configurations. Two classes of flow structures have been identified, characterized by pronouncedly different shock structures resulting from jet crossflow interactions. The injection angle and backward step height have been found to be the dominant design factors, while the other two play a subordinate role in fuel mixing for the configurations and variable ranges considered in this study. High injection angle and low step height are favored for higher total pressure saving and fuel penetration as well as enhanced fuel/air mixing at the downstream exit. However, lower injection angle and low step height may be preferred if priority is given to fuel mixing and flame holding in the recirculation region behind the backward step. Shock-tunnel experiments are planned by the authors in order to examine the insights gained through the present investigation.

## References

- [1] Paull, A., Alesi, H., and Anderson, S., "HyShot Flight Program and How it was Developed", AIAA Paper 2002-5248, Sep 2002.
- [2] Boyce, R. R., Gerard, S., and Paull, A., "The HyShot Scramjet Flight Experiment – flight data and CFD calculations compared", AIAA Paper 2003-7029, Dec 2003.
- [3] McClinton, C. R., "X-43 – Scramjet Power Breaks the Hypersonic Barrier: Dryden Lecture-ship in Research for 2006", AIAA Paper 2006-1-317, Jan 2006.
- [4] Boeing, "X-51A WaveRider Breaks Record in 1st Flight", <http://boeing.mediaroom.com>, May 2010.
- [5] Stalker, R. J., Paull, A., Mee, D. J., Morgan, R. G., and Jacobs, P. A., "Scramjets and shock tunnels – The Queensland experience", *Progress in Aerospace Sciences*, Vol. 41, 2005, pp.471-513.
- [6] Ferri, A., "Mixing-Controlled Supersonic Combustion", *Annual Review of Fluid Mechanics*, Vol. 5, No. 1, 1973, pp. 301-338.
- [7] Wendt, M. N., and Stalker, R. J., "Transverse and Parallel Injection of Hydrogen with Supersonic Combustion in a Shock Tunnel", *Shock Waves*, Vol. 6, 1996, pp. 53-59.
- [8] Lee, S. H. and Mitani, T., "Mixing Augmentation of Transverse Injection in Scramjet Combustor", *Journal of Propulsion and Power*, Vol. 19, No. 1, 2003, pp. 115-124.
- [9] Tomioka, S., Jacobsen, L. S., and Schetz, J. A., "Sonic Injection from Diamond-Shaped Orifices into a Supersonic Crossflow", *Journal of Propulsion and Power*, Vol. 19, No. 1, 2003, pp. 104-114.
- [10] Sunami, T. and Scheel, F., "Observation of Mixing and Combustion Process of H<sub>2</sub> Jet Injected into Supersonic Streamwise Vortices", *Shock Waves*, Springer-Verlag Berlin Heidelberg, 2005, pp. 921-926.
- [11] Kodera, M., Sunami, T., and Scheel, F., "Numerical Study on the Supersonic Mixing Enhancement Using Streamwise Vortices", AIAA Paper 2002-5117, Sep-Oct 2002.
- [12] Waitz, I. A., Qiu, Y. J., Manning, T. A., Fung, A. K. S., Elliot, J. K., Kerwin, J. M., Krasnodebski, J. K., O'Sullivan, M. N., Tew, D. E., Greitzer, E. M., Marble, F. E., Tan, C. S., and Tillman, T. G., "Enhanced Mixing with Streamwise Vorticity", *Progress in Aerospace Sciences*, Vol. 33, 1997, pp.323-351.
- [13] Karagozian, A., Wang, K., Le, A., and Smith, O., "Transverse Gas Jet Injection Behind a Rearward-Facing Step", *Journal of Propulsion and Power*, Vol. 12, No. 6, 1996, pp. 1129-1136.
- [14] Takahashi, S., Yamano, G., Wakai, K., Tsue, M., and Kono, M., "Self-Ignition and Transition to Flame-Holding in a Rectangular Scramjet Combustor with a Backward Step", *Proceedings of the Combustion Institute*, Vol. 28, No. 1, 2000, pp. 705-712.
- [15] Kuratani, N., Ikeda, Y., Nakajima, T., Tomioka, S., and Mitani, T., "Mixing Characteristics of Normal Injection into a Supersonic Backward-Facing Step Flow Measured with PIV", AIAA Paper 2002-237, Jan 2002.

- [16] Wu, J., Wang, H., Sun, M., Zhang, S., and Wang, Z., "Mixing Characteristics of Transverse Jet Injection into Supersonic Flow after Rearward-Facing Step", *Advances in Mechanical Engineering*, Vol. 2013, Article ID 762595, 7 pages, 2013.
- [17] Wen, C. Y., Chang, Y. C., Su, Y. H., and Yuan, H. F., "The Effect of the Recombination Shock behind a Backward Step on the Mixing Characteristics of an Inclined Sonic Methane Jet in a Supersonic Crossflow", ISSW Paper 0246-000284, Jul 2013.
- [18] Ogawa, H. and Boyce, R. R., "Physical Insight into Scramjet Inlet Behavior via Multi-Objective Design Optimization", *AIAA Journal*, Vol. 50, No. 8, 2012, pp. 1773-1783.
- [19] Ogawa, H. and Boyce, R. R., "Nozzle Design Optimization for Axisymmetric Scramjets by Using Surrogate-Assisted Evolutionary Algorithms", *Journal of Propulsion and Power*, Vol. 28, No. 6, 2012, pp. 1324-1338.
- [20] Ogawa, H. and Boyce, R. R., "Multi-Objective Design Optimization of Fuel Injection for Mixing Enhancement in Scramjets by Using Surrogate-Assisted Evolutionary Algorithms", AIAA Paper 2012-5815, Sep 2012.
- [21] Ogawa, H. and Boyce, R. R., "Computational Investigation of Fuel Injection with Various Injector Geometries and Mixing into Hypersonic Crossflow in Scramjet Engines", AIAA Paper 2013-0115, Jan 2013.
- [22] CFD++, *Software Package*, Ver.12.1, Metacomp Technologies Inc., CA, 2012.
- [23] Pointwise, *Software Package*, Ver.17.1, Pointwise Inc., TX, 2013.
- [24] Ray, T. and Smith, W., "A Surrogate Assisted Parallel Multiobjective Evolutionary Algorithm for Robust Engineering Design", *Engineering Optimization*, Vol.38, No.8, 2006, pp.997-1011.
- [25] Ray, T., Isaacs, A., and Smith, W., "Multi-objective optimization using surrogate assisted evolutionary algorithm", (*Introduction G.P.Rangaiah*), *Multi-objective Optimization: Techniques and Applications in Chemical Engineering*, World Scientific, Singapore, 2008, pp.131-151.
- [26] Queipo, N. V., Haftka, R. T., Shyy, W., Goel, T., Vaidyanathan, R., and Tucker, P. K., "Surrogate-based analysis and optimization", *Progress in Aerospace Sciences*, Vol.41, 2005, pp.1-28.
- [27] Alsumait, J. S., Sykulski, J. K., and Al-Othman, A. K., "A Hybrid GA-PS-SQP Method to Solve Power System Valve-Point Economic Dispatch Problems", *Applied Energy*, Vol. 87, No. 5, 2010, pp. 1773-1781.
- [28] Li, H. and Landa-Silva, D., "An Adaptive Evolutionary Multi-Objective Approach Based on Simulated Annealing", *Evolutionary Computation*, Vol. 19, No. 4, 2011, pp. 561-595.
- [29] Saltelli, A., "Making best use of model evaluations to compute sensitivity indices", *Computer Physics Communications*, Vol. 145, No. 2, 2002, pp. 280-297.
- [30] Saltelli, A., Ratto, M., Andres, T., Compolongo, F., Cariboni, J., Gatelli, D., Saisana, M., and Tarantola, S., *Global Sensitivity Analysis. The Primer*, Wiley, England, 2008.
- [31] Gruber, M. R., Nejad, A. S., Chen, T. H., and Dutton, J. C., "Mixing and Penetration Studies of Sonic Jets in a Mach 2 Freestream", *Journal of Propulsion and Power*, Vol. 11, No. 2, 1995, pp. 315-323.

## 5 Acknowledgements

The authors are grateful to A/Prof. T. Ray and Dr. A. Isaacs at UNSW Canberra for providing the MDO framework developed in the group. We wish to acknowledge the support of the Australian Research Council through the DECRA (Discovery Early Career Researcher Award) Grant No. DE120102277 for Dr. Ogawa.

## 6 Contact Author Email Address

mailto: [hideaki.ogawa@rmit.edu.au](mailto:hideaki.ogawa@rmit.edu.au)

## Copyright Statement

The authors confirm that they, and/or their company or organization, hold copyright on all of the original material included in this paper. The authors also confirm that they have obtained permission, from the copyright holder of any third party material included in this paper, to publish it as part of their paper. The authors confirm that they give permission, or have obtained permission from the copyright holder of this paper, for the publication and distribution of this paper as part of the ICAS 2014 proceedings or as individual off-prints from the proceedings.